
ω GNNs: DEEP GRAPH NEURAL NETWORKS ENHANCED BY MULTIPLE PROPAGATION OPERATORS

Moshe Eliasof

Department of Computer Science
Ben-Gurion University
Beer-Sheva, Israel
eliasof@post.bgu.ac.il

Lars Ruthotto

Department of Mathematics
Emory University
Atlanta, Georgia, USA
lruthotto@emory.edu

Eran Treister

Department of Computer Science
Ben-Gurion University
Beer-Sheva, Israel
erant@cs.bgu.ac.il

ABSTRACT

Graph Neural Networks (GNNs) are limited in their propagation operators. These operators often contain non-negative elements only and are shared across channels and layers, limiting the expressiveness of GNNs. Moreover, some GNNs suffer from over-smoothing, limiting their depth. On the other hand, Convolutional Neural Networks (CNNs) can learn diverse propagation filters, and phenomena like over-smoothing are typically not apparent in CNNs. In this paper, we bridge this gap by incorporating trainable channel-wise weighting factors ω to learn and mix multiple smoothing and sharpening propagation operators at each layer. Our generic method is called ω GNN, and we study two variants: ω GCN and ω GAT. For ω GCN, we theoretically analyse its behaviour and the impact of ω on the obtained node features. Our experiments confirm these findings, demonstrating and explaining how both variants do not over-smooth. Additionally, we experiment with 15 real-world datasets on node- and graph-classification tasks, where our ω GCN and ω GAT perform better or on par with state-of-the-art methods.

1 INTRODUCTION

Graph Neural Networks (GNNs) are useful for a wide array of fields, from computer vision and graphics (Monti et al., 2017; Wang et al., 2018; Eliasof & Treister, 2020) and social network analysis (Kipf & Welling, 2016; Defferrard et al., 2016) to bio-informatics (Hamilton et al., 2017; Jumper et al., 2021). Most GNNs are defined by applications of propagation and point-wise operators, where the former is often fixed and based on the graph Laplacian (e.g., GCN (Kipf & Welling, 2016)), or is defined by an attention mechanism (Veličković et al., 2018; Kim & Oh, 2021; Brody et al., 2022).

Most recent GNNs follow a general structure that involves two main ingredients – the propagation operator, denoted by $\mathbf{S}^{(l)}$, and a 1×1 convolution denoted by $\mathbf{K}^{(l)}$, as follows

$$\mathbf{f}^{(l+1)} = \sigma(\mathbf{S}^{(l)} \mathbf{f}^{(l)} \mathbf{K}^{(l)}), \quad (1)$$

where $\mathbf{f}^{(l)}$ denotes the feature tensor at the l -th layer. The main limitation of the above formulation is that the propagation operators in most common architectures are constrained to be non-negative. This leads to two drawbacks. First, this limits the expressiveness of GNNs. For example, the gradient of given graph node features can not be expressed by a non-negative operator, while a mixed-sign operator as in our proposed method can (see demonstrations in Fig. 1 and Fig. 2). Moreover, the utilization of strictly non-negative propagation operators yields a smoothing process, that may lead GNNs to suffer from over-smoothing. That is, the phenomenon where node features become indistinguishable from one and other as more GNN layers are stacked – causing severe performance degradation in deep GNNs (Li et al., 2018; Wu et al., 2019; Wang et al., 2019).

Both of the drawbacks mentioned above are not evident in Convolutional Neural Networks (CNNs), which can be interpreted as structured versions of GNNs (i.e., GNNs operating on a regular grid). The structured convolutions in CNNs allow to learn diverse propagation operators, and in particular it is known that mixed-sign kernels like sharpening filters are useful feature extractors in CNNs (Krizhevsky et al., 2012), and such operators cannot be obtained by non-negative (smoothing) kernels only. In the context of GNNs, Eliasof et al. (2022) have shown the significance and benefit of employing mixed-sign propagation operators in GNNs as well. In addition, the over-smoothing phenomenon is typically not evident in standard CNNs where the propagation (spatial) filters are learnt, and usually adding more layers improves accuracy (He et al., 2016). The discussion above demonstrates two gaps between CNNs and GNNs that we seek to bridge in this work.

A third gap between GNNs and CNNs is the ability of the latter to learn and mix multiple propagation operators. In the scope of separable convolutions, CNNs typically learn a distinct kernel per channel, known as a depth-wise convolution (Sandler et al., 2018) – a key element in modern CNNs (Tan & Le, 2019; Liu et al., 2022). On the contrary, the propagation operator $\mathbf{S}^{(l)}$ from equation 1 acts on all channels (Chen et al., 2020b; Veličković et al., 2018), and in some cases on all layers (Kipf & Welling, 2016; Wu et al., 2019). We note that one exception is the multi-head GAT (Veličković et al., 2018) where several attention heads are learnt per layer. However, this approach typically employs only a few heads due to the high computational cost and is still limited by learning non-negative propagation operators only.

In this paper we propose an effective modification to GNNs to directly address the three shortcomings of GNNs discussed above, by introducing a parameter ω to control the contribution and type of the propagation operator. We call our general approach ω GNN, and utilize GCN (Kipf & Welling, 2016) and GAT (Veličković et al., 2018) to construct two variants, ω GCN and ω GAT. We theoretically prove and empirically demonstrate that our ω GNN can prevent over-smoothing. Secondly, we show that by learning ω , our ω GNNs can yield propagation operators with mixed signs, ranging from smoothing to sharpening operators which do not exist in current GNNs (see Fig. 1 for an illustration). This approach enhances the expressiveness of the network, as demonstrated in Fig. 2, and to the best of our knowledge, was not considered in the GNNs mentioned above that employ non-negative propagation operators only. Lastly, we propose and demonstrate that by learning different ω per layer and channel, similarly to a depth-wise convolution in CNNs, our ω GNNs obtains state-of-the-art accuracy.

Our contributions are summarized as follows:

- We propose ω GNN, an effective and computationally light modification to GNNs of a common and generic structure, that directly avoids over-smoothing and enhances the expressiveness of GNNs. Our method is demonstrated by ω GCN and ω GAT.
- A theoretical analysis and experimental validation of the behaviour of ω GNN are provided to expose its improved expressiveness compared to standard propagation operators in GNNs.
- We propose to learn multiple propagation operators by learning ω *per layer and per channel* and mixing them using a 1×1 convolution to enhance the performance of GNNs.
- Our experiments with 15 real-world datasets on numerous applications and settings, from semi- and fully-supervised node classification to graph classification show that our ω GCN and ω GAT read on par or better performance than current state-of-the-art methods.

2 METHOD

We start by providing the notations that will be used throughout this paper, and displaying our general ω GNN in Sec. 2.1. Then we consider two popular GNNs that adhere to the structure presented in equation 1, namely GCN and GAT. We formulate and analyse the behaviour of their two counterparts ω GCN and ω GAT in Sec. 2.2 and 2.3, respectively.

Notations. Assume we are given an undirected graph defined by the set $\mathcal{G} = (\mathcal{V}, \mathcal{E})$ where \mathcal{V} is a set of n vertices and \mathcal{E} is a set of m edges. Let us denote by $\mathbf{f}_i \in \mathbb{R}^c$ the feature vector of the i -th node of \mathcal{G} with c channels. Also, we denote the adjacency matrix \mathbf{A} , where $\mathbf{A}_{ij} = 1$ if there exists an edge $(i, j) \in \mathcal{E}$ and 0 otherwise. We also define the diagonal degree matrix \mathbf{D} where \mathbf{D}_{ii} is the degree of

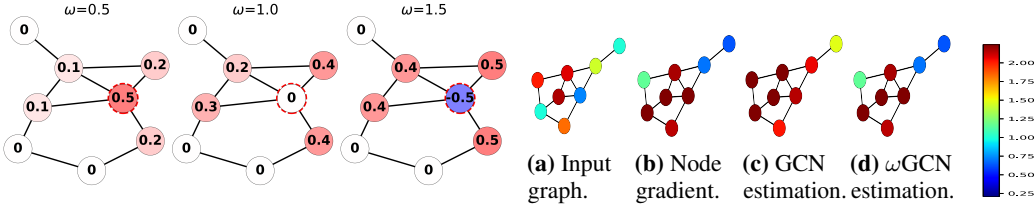


Figure 1: The impulse response of ω GCN’s propagation operator for different ω values. For $\omega = 0.5, 1.0$ non-negative values are obtained, while for $\omega = 1.5$ we see mixed-sign values. The dashed node starts from a feature of 1 and the rest with 0.

Figure 2: The expressiveness of ω GNNs. Our ω GCN can express the gradient of the node features while GCN cannot.

the i -th node. The graph Laplacian is given by $\mathbf{L} = \mathbf{D} - \mathbf{A}$. Let us also denote the adjacency and degree matrices with added self-loops by $\tilde{\mathbf{A}}$ and $\tilde{\mathbf{D}}$, respectively. Lastly, we denote the symmetrically normalized graph Laplacian by $\tilde{\mathbf{L}}^{sym} = \tilde{\mathbf{D}}^{-\frac{1}{2}} \tilde{\mathbf{L}} \tilde{\mathbf{D}}^{-\frac{1}{2}}$ where $\tilde{\mathbf{L}} = \tilde{\mathbf{D}} - \tilde{\mathbf{A}}$.

2.1 ω GNNs

The goal of ω GNNs is to utilize learnable mixed-sign propagation operators that control smoothing and sharpening to enrich GNNs expressiveness. Below, we describe how the learnt ω influences the obtained operator and how to learn and mix multiple operators for enhanced expressiveness.

Learning propagation weight ω . To address the expressiveness and over-smoothing issues, we suggest a general form given an arbitrary non-negative and normalized (e.g., such that its row sums equal to 1) propagation operator $\mathbf{S}^{(l)}$. Our general ω GNN is then given by

$$\mathbf{f}^{(l+1)} = \sigma \left(\left(\mathbf{I} - \omega^{(l)} \left(\mathbf{I} - \mathbf{S}^{(l)} \right) \right) \mathbf{f}^{(l)} \mathbf{K}^{(l)} \right), \quad (2)$$

where $\omega^{(l)}$ is a scalar that is learnt per layer, and in the next paragraph we offer a more elaborated version with a parameter ω per layer and channel. The introduction of $\omega^{(l)}$ allows our ω GNN layer to behave in a three-fold manner. When $\omega^{(l)} \leq 1$, a smoothing process is obtained¹. Note, that for $\omega^{(l)} = 1$, equation 2 reduces to the standard GNN dynamics from equation 1. In case $\omega^{(l)} = 0$, equation 2 reduces to a 1×1 convolution followed by a non-linear activation function, and does not propagate neighbouring node features. On the other hand, if $\omega^{(l)} > 1$, we obtain an operator with negative signs on the diagonal but positive on the off-diagonal entries, inducing a sharpening operator. An example of various $\omega^{(l)}$ values and their impulse response is given in Fig. 1. Thus, a learnable $\omega^{(l)}$ allows to learn a new family of operators, namely sharpening operators, that are not achieved by methods like GCN and GAT. To demonstrate the importance of sharpening operators, we consider a synthetic task of node gradient feature regression, given a graph and input node features (see Appendix B for more details). As depicted in Fig. 2, using a non-negative operator as in GCN cannot accurately express the gradient operator output, while our ω GCN estimates the gradient output with a machine precision accuracy. Also, the benefit of employing both smoothing and sharpening operators is reflected in the obtained accuracy of our method on real-world datasets in Sec. 4.

Multiple propagation operators. To learn multiple propagation operators, we extend equation 2 from a channels-shared weight to channel-wise weights by learning a vector $\vec{\omega}^{(l)} \in \mathcal{C}$ as follows

$$\mathbf{f}^{(l+1)} = \sigma \left(\left(\mathbf{I} - \boldsymbol{\Omega}_{\vec{\omega}^{(l)}} \left(\mathbf{I} - \mathbf{S}^{(l)} \right) \right) \mathbf{f}^{(l)} \mathbf{K}^{(l)} \right), \quad (3)$$

where $\boldsymbol{\Omega}_{\vec{\omega}^{(l)}}$ is an operator that scales each channel j with a different $\omega_j^{(l)}$. As discussed in Sec. 1, this procedure yields a propagation operator per-channel, which is similar to depth-wise convolutions

¹The use of the value 1 in this discussion corresponds to a non-negative operator $\mathbf{S}^{(l)}$ with zeros on its diagonal, normalized to have row sums of 1. Other normalizations may yield other constants. Also, if $0 < \mathbf{S}_{ii}^{(l)} < 1$, then setting $\omega^{(l)} > \frac{1}{1 - \mathbf{S}_{ii}^{(l)}}$ flips the sign of the i -th diagonal entry.

in CNNs (Howard et al., 2017; Sandler et al., 2018). Thus, the extension to a vector $\bar{\omega}^{(l)}$ helps to further bridge the gap between GNNs and CNNs.

We note that using this approach, our ω GNN is suitable to many existing GNNs, and in particular to those which act as a separable convolution, as described in equation 1. In what follows, we present and analyse two variants based on GCN and GAT, called ω GCN and ω GAT, respectively.

2.2 ω GCN

GCNs are a class of GNNs that employ a pre-determined propagation operator $\tilde{\mathbf{P}} = \tilde{\mathbf{D}}^{-\frac{1}{2}} \tilde{\mathbf{A}} \tilde{\mathbf{D}}^{-\frac{1}{2}}$, that stems from the graph Laplacian. For instance, GCN Kipf & Welling (2016) is given by:

$$\mathbf{f}^{(l+1)} = \sigma(\tilde{\mathbf{P}} \mathbf{f}^{(l)} \mathbf{K}^{(l)}), \quad (4)$$

that is, by setting $\mathbf{S}^{(l)} = \tilde{\mathbf{P}}$ in equation 1. Other methods like SGC (Wu et al., 2019), GCNII (Chen et al., 2020b) and EGNN (Zhou et al., 2021) also rely on $\tilde{\mathbf{P}}$ as a propagation operator.

The operator $\tilde{\mathbf{P}}$ is a fixed non-negative smoothing operator, hence, repeated applications of equation 4 lead to the over-smoothing phenomenon, where the feature maps converge to a single eigenvector as shown by Wu et al. (2019); Wang et al. (2019). Moreover, $\tilde{\mathbf{P}}$ is pre-determined, and solely depends on the graph connectivity, disregarding the node features, which may harm performance.

By baking our proposed ω GNN with a learnable weight, denoted by $\omega^{(l)} \in \mathbb{R}$ into GCN we obtain the following propagation scheme, named ω GCN:

$$\mathbf{f}^{(l+1)} = \sigma\left(\left(\mathbf{I} - \omega^{(l)}\left(\mathbf{I} - \tilde{\mathbf{P}}\right)\right) \mathbf{f}^{(l)} \mathbf{K}^{(l)}\right). \quad (5)$$

We now present theoretical analyses of our ω GCN and reason about its *non* over-smoothing property. We first define the node features Dirichlet energy at the l -th layer, as in Zhou et al. (2021):

$$E(\mathbf{f}^{(l)}) = \sum_{i \in \mathcal{V}} \sum_{j \in \mathcal{N}_i} \frac{1}{2} \left\| \frac{\mathbf{f}_i^{(l)}}{\sqrt{1+d_i}} - \frac{\mathbf{f}_j^{(l)}}{\sqrt{1+d_j}} \right\|_2^2. \quad (6)$$

Fig. 3a demonstrates how the Dirichlet energy $E(\mathbf{f}^{(l)})$ decays to zero when ω is a constant, and to a fixed positive value when ω is learnt. Next, we provide a theorem that characterizes the behaviour of ω and how it prevents over-smoothing. To this end we denote the propagation operator of ω GCN from equation 5 by

$$\tilde{\mathbf{P}}_\omega = \mathbf{I} - \omega \left(\mathbf{I} - \tilde{\mathbf{P}} \right) = \mathbf{I} - \omega \left(\mathbf{I} - \tilde{\mathbf{D}}^{-\frac{1}{2}} \tilde{\mathbf{A}} \tilde{\mathbf{D}}^{-\frac{1}{2}} \right) = \mathbf{I} - \omega \tilde{\mathbf{D}}^{-\frac{1}{2}} \mathbf{L} \tilde{\mathbf{D}}^{-\frac{1}{2}}, \quad (7)$$

where the latter equality is shown in Appendix A. In essence, we show that repeatedly applying the operator $\tilde{\mathbf{P}}$ is equivalent to applying gradient descent steps for minimizing equation 6 with a learning rate ω . We build on the observation that smoothing is beneficial (Gasteiger et al., 2019; Chamberlain et al., 2021) and assume that there exists an optimal energy at the last layer that satisfies $0 < E_{opt}(\mathbf{f}^{(L)}) < E(\mathbf{f}^{(0)})$. Then, we show that if we learn a single $\omega^{(l)} = \omega > 0$, shared across all layers, then taking L to infinity will lead ω to zero. Thus, our ω GCN will not over-smooth, as the energy at the last layer $E(\mathbf{f}^{(L)})$ can reach to $E_{opt}(\mathbf{f}^{(L)})$. Later, in Corollary 1.1, we generalize this result for a per-layer $\omega^{(l)}$, and empirically validate both results in Sec. 4.5. The proofs for the Theorem and Corollary below are given in Appendix A.

Theorem 1. Consider L applications of equation 7, i.e., $\mathbf{f}^{(L)} = (\tilde{\mathbf{P}}_\omega)^L \mathbf{f}^{(0)}$ with a shared parameter $\omega^{(l)} = \omega$ that is used in all the layers. Also assume that there is some optimal Dirichlet energy of the final feature map that satisfies $0 < E_{opt}(\mathbf{f}^{(L)}) < E(\mathbf{f}^{(0)})$. Then, at the limit, as more layers are added, ω converges to $\bar{\omega}/L$ up to first order accuracy, where L is the number of layers and $\bar{\omega}$ is a value that is independent of L and leads to E_{opt} .

Corollary 1.1. Allowing a variable $\omega^{(l)} > 0$ at each layer in Theorem 1, yields $\sum_{l=0}^{L-1} \omega^{(l)} = \bar{\omega}$ up to first order accuracy.

Next, we dwell on the second mechanism in which ω GCN prevents over-smoothing. We analyse the eigenvectors of $\tilde{\mathbf{P}}_\omega$, showing that different choices of ω yield different leading eigenvectors that alter the behaviour of the propagation operator (i.e. smoothing and sharpening processes). This result is useful because changing the leading eigenvector prevents the gravitation towards a specific eigenvector, which causes the over-smoothing to occur (Wu et al., 2019; Oono & Suzuki, 2020).

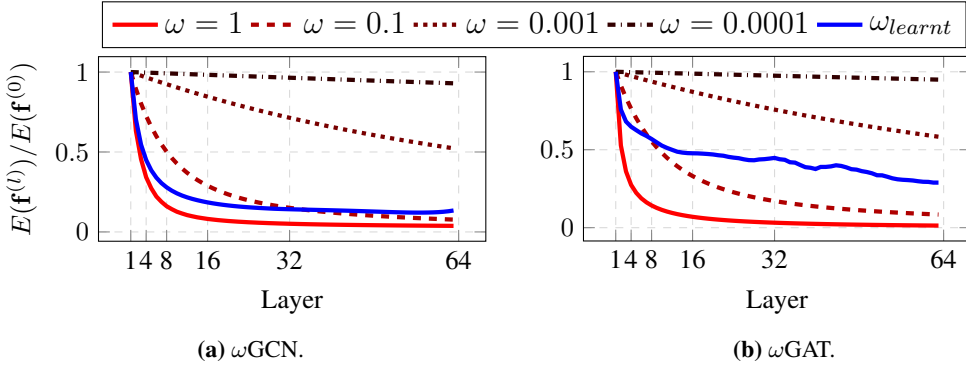


Figure 3: Node features energy at the l -th layer relative to the initial node embedding energy on Cora. Both ω GCN and ω GAT control the respective energies from equation 6 and equation 11 to avoid over-smoothing, while the baselines with $\omega = 1$ reduce the energies to 0 and over-smooth.

Theorem 2. Assume that the graph is connected. Then, there exists some $\omega_0 \geq 1$ where for all $0 < \omega < \omega_0$, the operator $\tilde{\mathbf{P}}_\omega$ in equation 7 is smoothing and the leading eigenvector is $\tilde{\mathbf{D}}^{\frac{1}{2}}\mathbf{1}$. For $\omega > \omega_0$ or $\omega < 0$, the leading eigenvector changes.

The proof for the theorem is given in Appendix A.

ω GCN with multiple propagation operators. To further increase the expressiveness of our ω GCN we extend $\omega^{(l)} \in \mathbb{R}$ to $\tilde{\omega}^{(l)} \in \mathbb{R}^c$ and learn a propagation operator per channel, at each layer. To this end, we modify equation 5 to the following formulation

$$\mathbf{f}^{(l+1)} = \sigma \left(\left(\mathbf{I} - \Omega_{\tilde{\omega}^{(l)}} \left(\mathbf{I} - \tilde{\mathbf{P}} \right) \right) \mathbf{f}^{(l)} \mathbf{K}^{(l)} \right). \quad (8)$$

As we show in Sec. 4.5, learning a propagation operator per channel is beneficial to improve accuracy.

2.3 ω GAT

The seminal GAT (Veličković et al., 2018) learns a non-negative edge-weight as follows

$$\alpha_{ij}^{(l)} = \frac{\exp \left(\text{LeakyReLU} \left(\mathbf{a}^{(l)\top} [\mathbf{W}^{(l)} \mathbf{f}_i^{(l)} || \mathbf{W}^{(l)} \mathbf{f}_j^{(l)}] \right) \right)}{\sum_{p \in \mathcal{N}_i} \exp \left(\text{LeakyReLU} \left(\mathbf{a}^{(l)\top} [\mathbf{W}^{(l)} \mathbf{f}_i^{(l)} || \mathbf{W}^{(l)} \mathbf{f}_p^{(l)}] \right) \right)}, \quad (9)$$

where $\mathbf{a}^{(l)} \in \mathbb{R}^{2c}$ and $\mathbf{W}^{(l)} \in \mathbb{R}^{c \times c}$ are trainable parameters and $||$ denotes channel-wise concatenation. Here, GAT is obtained by defining the propagation operator $\mathbf{S}^{(l)}$ in equation 1 as $\hat{\mathbf{S}}_{ij}^{(l)} = \alpha_{ij}^{(l)}$.

To avoid repeated equations, we skip the per-layer ω formulation (as in equation 2) and directly define the per-channel ω GAT as follows

$$\mathbf{f}^{(l+1)} = \sigma \left(\left(\mathbf{I} - \Omega_{\tilde{\omega}^{(l)}} \left(\mathbf{I} - \hat{\mathbf{S}}^{(l)} \right) \right) \mathbf{f}^{(l)} \mathbf{K}^{(l)} \right). \quad (10)$$

The introduction of $\Omega_{\tilde{\omega}^{(l)}}$ yields a learnable propagation operator per layer and channel. We note that it is also possible to obtain multiple propagation operators from GAT by using a multi-head attention. However, we distinguish our proposition from GAT in a 2-fold fashion. First, our propagation operators belong to a broader family that includes smoothing and sharpening operators as opposed to smoothing-only due to the SoftMax normalization in GAT. Secondly, our method requires less computational overhead when adding more propagation operators, as our ω GAT requires a scalar per operator, while GAT doubles the number of channels to obtain more attention-heads. Also, utilizing a multi-head GAT can still lead to over-smoothing, as all the heads induce a non-negative operator.

To study the behaviour of our ω GAT, we inspect its node features energy compared to GAT. To this end, we define the GAT energy as

$$E_{\text{GAT}}(\mathbf{f}^{(l)}) = \sum_{i \in \mathcal{V}} \sum_{j \in \mathcal{N}_i} \frac{1}{2} \|\mathbf{f}_i^{(l)} - \mathbf{f}_j^{(l)}\|_2^2. \quad (11)$$

This modification of the Dirichlet energy from equation 6 is required because in GAT (Veličković et al., 2018) the leading eigenvector of the propagation operator $\hat{\mathbf{S}}^{(l)}$ is the constant vector $\mathbf{1}$ as shown by Chen et al. (2020a), unlike the vector $\tilde{\mathbf{D}}^{\frac{1}{2}}\mathbf{1}$ in the symmetric normalized $\tilde{\mathbf{P}}$ from GCN (Kipf & Welling, 2016) where the Dirichlet energy is natural to consider (Pei et al., 2020).

We present the energy of a 64 layer GAT trained on the Cora dataset in Fig. 3b. It is evident that the accuracy degradation of a deep GAT reported by Zhao & Akoglu (2020) is in congruence with the decaying energy in equation 11, while our ω GAT does not experience decaying energy nor accuracy degradation as more layers are added, as can be seen in Tab. 2. To further validate our findings, we repeat this experiment in Appendix D on additional datasets and reach to the same conclusion.

2.4 COMPUTATIONAL COSTS

Our ω GNN approach is general and can be applied to any GNN that conforms to the structure of equation 1 and can be modified into equation 3. The additional parameters compared to the baseline GNN are the added $\Omega_{\tilde{\omega}^{(l)}} \in \mathbb{R}^c$ parameters at each layer, yielding a relatively low computational overhead. For example, in GCN (Kipf & Welling, 2016) there are $c \times c$ trainable parameters requiring $c \times c \times n$ multiplications due to the 1×1 convolution $\mathbf{K}^{(l)}$. In our ω GCN, we will have $c \times c + c$ parameters and $(c + 1) \times c \times n$ multiplications. That is in addition to applying the propagation operators $\mathbf{S}^{(l)}$, which are identical for both methods. A similar analysis holds for GAT. To validate the actual complexity of our method, we present the training and inference times for ω GCN and ω GAT in Appendix G. We see a negligible addition to the runtimes compared to the baselines, at the return of better performance.

3 OTHER RELATED WORK

Over-smoothing in GNNs. The over-smoothing phenomenon was identified by Li et al. (2018), and was profoundly studied in recent years. Various methods stemming from different approaches were proposed. For example, methods like DropEdge (Rong et al., 2020), PairNorm (Zhao & Akoglu, 2020), and EGNN (Zhou et al., 2021) propose augmentation, normalization and energy-based penalty methods to alleviate over-smoothing, respectively. Other methods like Min et al. (2020) propose to augment GCN with geometric scattering transforms and residual convolutions, and GCNII (Chen et al., 2020b) present a spectral analysis of the smoothing property of GCN (Kipf & Welling, 2016) and propose adding an initial identity residual connection and a decay of the weights of deeper layers, which are also used in EGNN (Zhou et al., 2021).

Graph Neural Diffusion. The view of GNNs as a diffusion process has gained popularity in recent years. Methods like APPNP (Klicpera et al., 2019) propose to use a personalized PageRank (Page et al., 1999) algorithm to determine the diffusion of features, and GDC (Gasteiger et al., 2019) imposes constraints on the ChebNet (Defferrard et al., 2016) architecture to obtain diffusion kernels, showing accuracy improvement. Other works like GRAND (Chamberlain et al., 2021), CFD-GCN (Belbute-Peres et al., 2020), PDE-GCN (Eliasof et al., 2021) and GRAND++ (Thorpe et al., 2022) propose to view GNN layers as time steps in the integration process of ODEs and PDEs that arise from a non-linear heat equation, allowing to control the diffusion (smoothing) in the network to prevent over-smoothing. In addition, some GNNs (Eliasof et al., 2021; Rusch et al., 2022) propose a mixture between diffusion and oscillatory processes to avoid over-smoothing by frequency preservation of the features.

Mixed-sign operators in GNNs. The importance of mixed-sign operators in GNNs was discussed in Eliasof et al. (2022), where k -hop filters and stochastic path sampling mechanisms are utilized. However, such a method requires significantly more computational resources than a standard GNN like Kipf & Welling (2016); Veličković et al. (2018) due to the path sampling strategy and larger filters of 5-hop required for optimal accuracy. However, our ω GNNs perform 1-hop convolutions and as we show in Appendix G, obtain state-of-the-art results without significant added computational costs.

Table 1: Summary of semi-supervised node classification accuracy (%)

Method	GCN	GAT	APPNP	GCNII	GRAND	superGAT	EGNN	ω GCN (Ours)	ω GAT (Ours)
Cora	81.1	83.1	83.3	85.5	84.7	84.3	85.7	85.9	84.8
Citeseer	70.8	70.8	71.8	73.4	73.6	72.6	—	73.3	74.0
Pubmed	79.0	78.5	80.1	80.3	71.0	81.7	80.1	81.1	81.8

Table 2: Semi-supervised node classification accuracy (%). — indicates not available results.

Dataset Layers	Cora						Citeseer						Pubmed					
	2	4	8	16	32	64	2	4	8	16	32	64	2	4	8	16	32	64
GCN	81.1	80.4	69.5	64.9	60.3	28.7	70.8	67.6	30.2	18.3	25.0	20.0	79.0	76.5	61.2	40.9	22.4	35.3
GCN (Drop)	82.8	82.0	75.8	75.7	62.5	49.5	72.3	70.6	61.4	57.2	41.6	34.4	79.6	79.4	78.1	78.5	77.0	61.5
JKNet	—	80.2	80.7	80.2	81.1	71.5	—	68.7	67.7	69.8	68.2	63.4	—	78.0	78.1	72.6	72.4	74.5
JKNet (Drop)	—	83.3	82.6	83.0	82.5	83.2	—	72.6	71.8	72.6	70.8	72.2	—	78.7	78.7	79.7	79.2	78.9
Incep	—	77.6	76.5	81.7	81.7	80.0	—	69.3	68.4	70.2	68.0	67.5	—	77.7	77.9	74.9	—	—
Incep (Drop)	—	82.9	82.5	83.1	83.1	83.5	—	72.7	71.4	72.5	72.6	71.0	—	79.5	78.6	79.0	—	—
GCNII	82.2	82.6	84.2	84.6	85.4	85.5	68.2	68.8	70.6	72.9	73.4	73.4	78.2	78.8	79.3	80.2	79.8	79.7
GCNII*	80.2	82.3	82.8	83.5	84.9	85.3	66.1	66.7	70.6	72.0	73.2	73.1	77.7	78.2	78.8	80.3	79.8	80.1
PDE-GCN _D	82.0	83.6	84.0	84.2	84.3	84.3	74.6	75.0	75.2	75.5	75.6	75.5	79.3	80.6	80.1	80.4	80.2	80.3
EGNN	83.2	—	—	85.4	—	85.7	—	—	—	—	—	—	79.2	—	—	80.0	—	80.1
ω GCN (Ours)	82.6	83.8	84.2	84.4	85.5	85.9	71.3	71.6	72.1	72.4	73.3	73.3	79.7	80.2	80.1	80.5	80.8	81.1
ω GAT (Ours)	83.4	83.7	84.0	84.3	84.4	84.8	72.5	73.1	73.3	73.5	73.9	74.0	80.3	81.0	81.2	81.3	81.5	81.8

4 EXPERIMENTS

We demonstrate our ω GCN and ω GAT on node classification, inductive learning and graph classification tasks. Additionally, we conduct an ablation study of the different configurations of our method and experimentally verify the theorems from Sec. 2. A description of the network architectures is given in Appendix E. We use the Adam (Kingma & Ba, 2014) optimizer in all experiments, and perform grid search to determine the hyper-parameters reported in Appendix F. The objective function in all experiments is the cross-entropy loss, besides inductive learning on PPI (Hamilton et al., 2017) where we use the binary cross-entropy loss. Our code is implemented with PyTorch (Paszke et al., 2019) and PyTorch-Geometric (Fey & Lenssen, 2019) and trained on an Nvidia Titan RTX GPU.

We show that for all the considered tasks and datasets, whose statistics are provided Appendix C, our ω GCN and ω GAT are either better or on par with other state-of-the-art models.

4.1 SEMI-SUPERVISED NODE CLASSIFICATION

We employ the Cora, Citeseer and Pubmed (Sen et al., 2008) datasets using the standard training/validation/testing split by Yang et al. (2016), with 20 nodes per class for training, 500 validation nodes and 1,000 testing nodes. We follow the training and evaluation scheme of Chen et al. (2020b) and compare with models like GCN, GAT, superGAT (Kim & Oh, 2021), Inception (Szegedy et al., 2017), APPNP (Klicpera et al., 2019), JKNet Xu et al. (2018), DropEdge (Rong et al., 2020), GCNII (Chen et al., 2020b), GRAND (Chamberlain et al., 2021), PDE-GCN (Eliasof et al., 2021) and EGNN (Zhou et al., 2021). We summarize the results in Tab. 1 where we see better or on par performance with other state-of-the-art methods. Additionally, we report the accuracy per number of layers, from 2 to 64 In Tab. 2, where it is evident that our ω GCN and ω GAT do not over-smooth. To ensure the robustness of our method, we also experiment with 100 random splits in Appendix I where our ω GCN and ω GAT continue to perform better or on par with state-of-the-art methods.

4.2 FULLY-SUPERVISED NODE CLASSIFICATION

To further validate the efficacy of our method on fully-supervised node classification, both on homophilic and heterophilic datasets as defined in Pei et al. (2020). Specifically, examine our ω GCN and ω GAT on Cora, Citeseer, Pubmed, Chameleon (Rozemberczki et al., 2021), Cornell, Texas and Wisconsin using the identical train/validation/test splits of 48%, 32%, 20%, respectively, and report

Table 3: Fully-supervised node classification accuracy (%). (L) denotes the number of layers.

Method	Cora	Cite.	Pubm.	Cham.	Corn.	Texas	Wisc.
GCN (Kipf & Welling, 2016)	85.77	73.68	88.13	28.18	52.70	52.16	45.88
GAT (Veličković et al., 2018)	86.37	74.32	87.62	42.93	54.32	58.38	49.41
Geom-GCN (Pei et al., 2020)	85.27	77.99	90.05	60.90	60.81	67.57	64.12
APPNP (Klicpera et al., 2019)	87.87	76.53	89.40	54.30	73.51	65.41	69.02
H2GCN (Zhu et al., 2020)	87.87	77.11	89.49	60.11	82.70	84.86	87.65
SD (Bodnar et al., 2022)	87.30	74.14	89.49	68.86	86.49	85.95	89.41
JKNet (Xu et al., 2018)	85.25 (16)	75.85 (8)	88.94 (64)	60.07 (32)	57.30 (4)	56.49 (32)	48.82 (8)
JKNet (Drop) (Rong et al., 2020)	87.46 (16)	75.96 (8)	89.45 (64)	62.08 (32)	61.08 (4)	57.30 (32)	50.59 (8)
Incep (Drop) (Rong et al., 2020)	86.86 (8)	76.83 (8)	89.18 (4)	61.71 (8)	61.62 (16)	57.84 (8)	50.20 (8)
GCNII (Chen et al., 2020b)	88.49 (64)	77.08 (64)	89.57 (64)	60.61 (8)	74.86 (16)	69.46 (32)	74.12 (16)
GCNII* (Chen et al., 2020b)	88.01 (64)	77.13 (64)	90.30 (64)	62.48 (8)	76.49 (16)	77.84 (32)	81.57 (16)
PDE-GCN _M (Eliasof et al., 2021)	88.60 (16)	78.48 (32)	89.93 (16)	66.01 (16)	89.73 (64)	93.24 (32)	91.76 (16)
ω GCN (Ours)	89.30 (16)	77.88 (16)	90.45 (8)	70.02 (16)	91.35 (32)	94.05 (32)	92.35 (32)
ω GAT (Ours)	89.25 (8)	78.01 (16)	90.65 (8)	72.23 (8)	91.62 (16)	94.59 (16)	92.94 (16)

Table 4: Fully-supervised node classification accuracy (%).

Method	Actor	Ogbn-arxiv
GCN (Kipf & Welling, 2016)	26.86	71.74
GAT (Veličković et al., 2018)	28.45	71.59
GATv2 (Brody et al., 2022)	—	71.87
APPNP (Klicpera et al., 2019)	31.26	71.82
Geom-GCN-P (Pei et al., 2020)	31.63	—
JKNet (Xu et al., 2018)	29.81	72.19
SGC (Wu et al., 2019)	30.98	69.20
GCNII (Chen et al., 2020b)	32.87	72.74
EGNN (Zhou et al., 2021)	—	72.70
GRAND (Chamberlain et al., 2021)	—	72.23
ω GCN (Ours)	38.94	73.02
ω GAT (Ours)	38.64	72.76

Table 5: Inductive learning on PPI dataset. Results are reported in micro-averaged F1 score.

Method	Micro-averaged F1
GCN Kipf & Welling (2016)	60.73
GraphSAGE Hamilton et al. (2017)	61.20
VR-GCN (Chen et al., 2018)	97.80
GaN (Zhang et al., 2018a)	98.71
GAT (Veličković et al., 2018)	97.30
JKNet (Xu et al., 2018)	97.60
GeniePath (Liu et al., 2018)	98.50
Cluster-GCN (Chiang et al., 2019)	99.36
GCNII* (Chen et al., 2020b)	99.58
PDE-GCN _M (Eliasof et al., 2021)	99.18
ω GCN (Ours)	99.60
ω GAT (Ours)	99.48

the average performance over 10 random splits from Pei et al. (2020). We compare our performance with, GCN, GAT, Geom-GCN, APPNP, JKNet, Inception, GCNII, PDE-GCN and others, as presented in Tab. 3. Additionally, we evaluate our ω GCN and ω GAT on the Actor (Rozemberczki et al., 2021) and Ogbn-arxiv (Hu et al., 2020) datasets, as reported in Tab. 4. We see an accuracy improvement across all benchmarks compared to the considered methods. In Appendix J we present and discuss the learnt $\vec{\omega}$ for homophilic and heterophilic datasets.

4.3 INDUCTIVE LEARNING

We employ the PPI dataset (Hamilton et al., 2017) for the inductive learning task. We use 8 layer ω GCN and ω GAT, with a learning rate of 0.001, dropout of 0.2 and no weight-decay. As a comparison we consider several methods and report the micro-averaged F1 score in Tab. 5. Our ω GCN achieves a score of 99.60, which is significantly superior than its baseline – GCN, and also performs better than methods like GAT, JKNet, GeniePath, Cluster-GCN and PDE-GCN.

4.4 GRAPH CLASSIFICATION

Previous experiments considered the *node-classification* task. To further demonstrate the efficacy of our ω GNNs we experiment with graph classification on TUDatasets (Morris et al., 2020). Here, we follow the same experimental settings from Xu et al. (2019), and report the 10 fold cross-validation performance on MUTAG, PTC, PROTEINS, NCI1 and NCI109 datasets. The hyper-parameters are determined by a grid search, as in Xu et al. (2019) and are reported in Appendix E. We compare our ω GCN and ω GAT with recent and popular methods like GIN (Xu et al., 2019), DGCNN (Zhang et al., 2018b), IGN (Maron et al., 2018), GSN (Bouritsas et al., 2022), SIN (Bodnar et al., 2021b), CIN (Bodnar et al., 2021a) and others. We also compare with methods that stem from 'classical'

Table 6: Graph classification accuracy (%) on TUDatasets (Morris et al., 2020).

Method	MUTAG	PTC	PROTEINS	NCI1	NCI109
RWK (Gärtner et al., 2003)	79.2 ± 2.1	55.9 ± 0.3	59.6 ± 0.1	—	—
GK (Shervashidze et al., 2009)	81.4 ± 1.7	55.7 ± 0.5	71.4 ± 0.3	62.5 ± 0.3	62.4 ± 0.3
PK (Neumann et al., 2016)	76.0 ± 2.7	59.5 ± 2.4	73.7 ± 0.7	82.5 ± 0.5	—
WL Kernel (Shervashidze et al., 2011)	90.4 ± 5.7	59.9 ± 4.3	75.0 ± 3.1	86.0 ± 1.8	—
DGCNN (Zhang et al., 2018b)	85.8 ± 1.8	58.6 ± 2.5	75.5 ± 0.9	74.4 ± 0.5	—
IGN (Maron et al., 2018)	83.9 ± 13.0	58.5 ± 6.9	76.6 ± 5.5	74.3 ± 2.7	72.8 ± 1.5
PPGNS (Maron et al., 2019)	90.6 ± 8.7	66.2 ± 6.6	77.2 ± 4.7	83.2 ± 1.1	82.2 ± 1.4
NATURAL GN (de Haan et al., 2020)	89.4 ± 1.6	66.8 ± 1.7	71.7 ± 1.0	82.4 ± 1.3	—
GSN (Bouritsas et al., 2022)	92.2 ± 7.5	68.2 ± 7.2	76.6 ± 5.0	83.5 ± 2.0	—
SIN (Bodnar et al., 2021b)	—	—	76.4 ± 3.3	82.7 ± 2.1	—
CIN (Bodnar et al., 2021a)	92.7 ± 3.6	68.2 ± 3.5	77.0 ± 3.4	83.6 ± 3.1	84.0 ± 3.1
GIN (Xu et al., 2019)	89.4 ± 5.6	64.6 ± 7.0	76.2 ± 2.8	82.7 ± 1.7	82.2 ± 1.6
GIN + ID (You et al., 2021)	90.4 ± 5.4	67.2 ± 4.3	75.4 ± 2.7	82.6 ± 1.6	82.1 ± 1.5
DROP (Rong et al., 2020)	91.0 ± 5.7	64.5 ± 2.6	73.5 ± 4.5	82.0 ± 2.6	82.2 ± 1.4
GCONV (Morris et al., 2019)	90.5 ± 4.6	64.9 ± 10.4	73.9 ± 6.1	82.4 ± 2.7	81.7 ± 1.0
RNI (Abboud et al., 2020)	91.0 ± 4.9	64.3 ± 6.1	73.3 ± 3.3	82.1 ± 1.7	81.7 ± 1.0
ω GCN (Ours)	94.6 ± 4.1	73.8 ± 4.3	80.2 ± 2.5	84.1 ± 1.2	84.5 ± 1.8
ω GAT (Ours)	95.2 ± 3.7	75.8 ± 3.5	80.7 ± 3.7	84.4 ± 1.7	83.6 ± 1.2

Table 7: Accuracy (%) of variants of ω GCN on semi-supervised classification.

Data.	Variant	Layers					
		2	4	8	16	32	64
Cora	ω GCN _G	83.4	84.3	84.2	84.1	84.3	84.4
	ω GCN _{PL}	83.0	83.6	84.0	84.2	84.5	84.8
	ω GCN	82.6	83.8	84.2	84.4	85.5	85.9
Cite.	ω GCN _G	71.0	71.4	71.3	71.7	72.0	71.8
	ω GCN _{PL}	71.1	71.3	71.5	71.8	72.4	72.6
	ω GCN	71.3	71.6	72.1	72.4	73.3	73.3
Pub.	ω GCN _G	79.8	80.4	80.5	80.4	80.2	80.3
	ω GCN _{PL}	79.8	80.0	80.2	80.4	80.5	80.8
	ω GCN	79.7	80.2	80.1	80.5	80.8	81.1

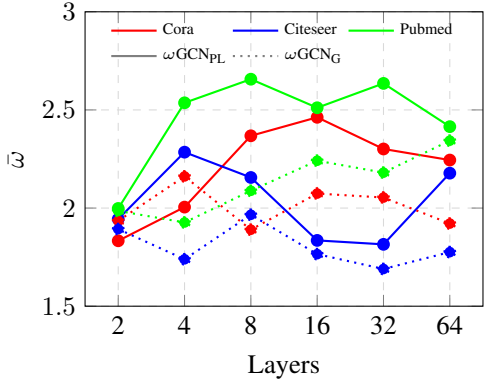


Figure 4: The summation of weighting factors $\bar{\omega}$ vs. the number layers for ω GCN_G and ω GCN_{PL}.

graph algorithms like RWK (Gärtner et al., 2003) and WL Kernel (Shervashidze et al., 2011). All the results are summarized in Tab. 6, with an evident improvement or similar results to current deep learning as well as classical methods, highlighting the efficacy of our approach.

4.5 ABLATION STUDY

In this section we study the different components and configurations of our ω GNN. We start by allowing a global (single) ω to be learnt throughout all the layers—this architecture is dubbed as ω GCN_G. We validate that this simple variant does not over-smooth, depicted in Tab. 7. The table also shows ω GCN_{PL}, that includes a single parameter $\omega^{(l)}$ per layer, and ω GCN shown in the results earlier that has $\Omega^{(l)}$, i.e., a parameter per layer and channel, which yields further accuracy improvements. In addition, we empirically verify our theoretical results from Sec. 2 in Fig. 4, where we show that $\bar{\omega} = L\omega$ and $\bar{\omega} = \sum_{l=0}^{L-1} \omega^{(l)}$ is similar for varying number of layers L as Theorem 1 and Corollary 1.1 suggest. For completeness, we also perform the ablation study on ω GAT in Appendix H.

5 SUMMARY

In this work we proposed an effective and computationally efficient modification that applies to a large family of GNNs that carry the form of a separable propagation and 1×1 convolutions, and in particular we demonstrate its efficacy on the popular GCN and GAT architectures. We provide theorems that reason about the smoothing nature of GCN and through the lens of operator analysis suggest to learn weighting factors $\vec{\omega}$ learn and mix smoothing and sharpening propagation operators. Through an extensive set of experiments on numerous datasets, ranging from node classification to graph classification, as well as an ablation study that validates our theoretical findings, we demonstrate the contribution of our ω GNN, reading on par or achieving new state-of-the-art performance.

REFERENCES

Ralph Abboud, Ismail Ilkan Ceylan, Martin Grohe, and Thomas Lukasiewicz. The surprising power of graph neural networks with random node initialization. *arXiv preprint arXiv:2010.01179*, 2020.

Filipe de Avila Belbute-Peres, Thomas D. Economon, and J. Zico Kolter. Combining Differentiable PDE Solvers and Graph Neural Networks for Fluid Flow Prediction. In *International Conference on Machine Learning (ICML)*, 2020.

Cristian Bodnar, Fabrizio Frasca, Nina Otter, Yuguang Wang, Pietro Lio, Guido F Montufar, and Michael Bronstein. Weisfeiler and lehman go cellular: Cw networks. *Advances in Neural Information Processing Systems*, 34:2625–2640, 2021a.

Cristian Bodnar, Fabrizio Frasca, Yuguang Wang, Nina Otter, Guido F Montufar, Pietro Lio, and Michael Bronstein. Weisfeiler and lehman go topological: Message passing simplicial networks. In *International Conference on Machine Learning*, pp. 1026–1037. PMLR, 2021b.

Cristian Bodnar, Francesco Di Giovanni, Benjamin Paul Chamberlain, Pietro Lio, and Michael M Bronstein. Neural sheaf diffusion: A topological perspective on heterophily and oversmoothing in gnns. *arXiv preprint arXiv:2202.04579*, 2022.

Giorgos Bouritsas, Fabrizio Frasca, Stefanos P Zafeiriou, and Michael Bronstein. Improving graph neural network expressivity via subgraph isomorphism counting. *IEEE Transactions on Pattern Analysis and Machine Intelligence*, 2022.

Shaked Brody, Uri Alon, and Eran Yahav. How attentive are graph attention networks? In *International Conference on Learning Representations*, 2022. URL <https://openreview.net/forum?id=F72ximsx7C1>.

Benjamin Paul Chamberlain, James Rowbottom, Maria Gorinova, Stefan Webb, Emanuele Rossi, and Michael M Bronstein. Grand: Graph neural diffusion. *arXiv preprint arXiv:2106.10934*, 2021.

Deli Chen, Yankai Lin, Wei Li, Peng Li, Jie Zhou, and Xu Sun. Measuring and relieving the over-smoothing problem for graph neural networks from the topological view. *Proceedings of the AAAI Conference on Artificial Intelligence*, 34:3438–3445, 04 2020a. doi: 10.1609/aaai.v34i04.5747.

Jianfei Chen, Jun Zhu, and Le Song. Stochastic training of graph convolutional networks with variance reduction. In Jennifer Dy and Andreas Krause (eds.), *Proceedings of the 35th International Conference on Machine Learning*, volume 80 of *Proceedings of Machine Learning Research*, pp. 942–950. PMLR, 10–15 Jul 2018. URL <http://proceedings.mlr.press/v80/chen18p.html>.

Ming Chen, Zhewei Wei, Zengfeng Huang, Bolin Ding, and Yaliang Li. Simple and deep graph convolutional networks. In Hal Daumé III and Aarti Singh (eds.), *Proceedings of the 37th International Conference on Machine Learning*, volume 119 of *Proceedings of Machine Learning Research*, pp. 1725–1735. PMLR, 13–18 Jul 2020b. URL <http://proceedings.mlr.press/v119/chen20v.html>.

Wei-Lin Chiang, Xuanqing Liu, Si Si, Yang Li, Samy Bengio, and Cho-Jui Hsieh. Cluster-gcn: An efficient algorithm for training deep and large graph convolutional networks. In *ACM SIGKDD Conference on Knowledge Discovery and Data Mining (KDD)*, 2019. URL <https://arxiv.org/pdf/1905.07953.pdf>.

Pim de Haan, Taco S Cohen, and Max Welling. Natural graph networks. *Advances in Neural Information Processing Systems*, 33:3636–3646, 2020.

Michaël Defferrard, Xavier Bresson, and Pierre Vandergheynst. Convolutional neural networks on graphs with fast localized spectral filtering. In *Advances in neural information processing systems*, pp. 3844–3852, 2016.

Moshe Eliasof and Eran Treister. Diffgcn: Graph convolutional networks via differential operators and algebraic multigrid pooling. *34th Conference on Neural Information Processing Systems (NeurIPS 2020), Vancouver, Canada.*, 2020.

Moshe Eliasof, Eldad Haber, and Eran Treister. Pde-gcn: Novel architectures for graph neural networks motivated by partial differential equations. *Advances in Neural Information Processing Systems*, 34, 2021.

Moshe Eliasof, Eldad Haber, and Eran Treister. pathgcn: Learning general graph spatial operators from paths. In *International Conference on Machine Learning*, pp. 5878–5891. PMLR, 2022.

Matthias Fey and Jan E. Lenssen. Fast graph representation learning with PyTorch Geometric. In *ICLR Workshop on Representation Learning on Graphs and Manifolds*, 2019.

Thomas Gärtner, Peter Flach, and Stefan Wrobel. On graph kernels: Hardness results and efficient alternatives. In *Learning theory and kernel machines*, pp. 129–143. Springer, 2003.

Johannes Gasteiger, Stefan Weißenberger, and Stephan Günnemann. Diffusion improves graph learning. In *Conference on Neural Information Processing Systems (NeurIPS)*, 2019.

Xavier Glorot and Yoshua Bengio. Understanding the difficulty of training deep feedforward neural networks. In *Proceedings of the thirteenth international conference on artificial intelligence and statistics*, pp. 249–256. JMLR Workshop and Conference Proceedings, 2010.

William L. Hamilton, Rex Ying, and Jure Leskovec. Inductive representation learning on large graphs. In *NIPS*, 2017.

Kaiming He, Xiangyu Zhang, Shaoqing Ren, and Jian Sun. Deep residual learning for image recognition. In *Proceedings of the IEEE Conference on Computer Vision and Pattern Recognition*, pp. 770–778, 2016.

Andrew G Howard, Menglong Zhu, Bo Chen, Dmitry Kalenichenko, Weijun Wang, Tobias Weyand, Marco Andreetto, and Hartwig Adam. MobileNets: Efficient convolutional neural networks for mobile vision applications. *arXiv preprint arXiv:1704.04861*, 2017.

Weihua Hu, Matthias Fey, Marinka Zitnik, Yuxiao Dong, Hongyu Ren, Bowen Liu, Michele Catasta, and Jure Leskovec. Open graph benchmark: Datasets for machine learning on graphs. *arXiv preprint arXiv:2005.00687*, 2020.

John Jumper, Richard Evans, Alexander Pritzel, Tim Green, Michael Figurnov, Olaf Ronneberger, Kathryn Tunyasuvunakool, Russ Bates, Augustin Žídek, Anna Potapenko, Alex Bridgland, Clemens Meyer, Simon A. A. Kohl, Andrew J. Ballard, Andrew Cowie, Bernardino Romera-Paredes, Stanislav Nikolov, Rishabh Jain, Jonas Adler, Trevor Back, Stig Petersen, David Reiman, Ellen Clancy, Michal Zielinski, Martin Steinegger, Michalina Pacholska, Tamas Berghammer, David Silver, Oriol Vinyals, Andrew W. Senior, Koray Kavukcuoglu, Pushmeet Kohli, and Demis Hassabis. Applying and improving alphafold at casp14. *Proteins*, 2021. ISSN 1097-0134. doi: 10.1002/prot.26257. _eprint: <https://onlinelibrary.wiley.com/doi/pdf/10.1002/prot.26257>.

Dongkwan Kim and Alice Oh. How to find your friendly neighborhood: Graph attention design with self-supervision. In *International Conference on Learning Representations*, 2021. URL <https://openreview.net/forum?id=Wi5KUN1qWty>.

Diederik P Kingma and Jimmy Ba. Adam: A method for stochastic optimization. *arXiv preprint arXiv:1412.6980*, 2014.

Thomas N Kipf and Max Welling. Semi-supervised classification with graph convolutional networks. *arXiv preprint arXiv:1609.02907*, 2016.

Johannes Klicpera, Aleksandar Bojchevski, and Stephan Günnemann. Combining neural networks with personalized pagerank for classification on graphs. In *International Conference on Learning Representations*, 2019. URL <https://openreview.net/forum?id=H1gL-2A9Ym>.

A. Krizhevsky, I. Sutskever, and G. Hinton. Imagenet classification with deep convolutional neural networks. *Adv Neural Inf Process Syst*, 61:1097–1105, 2012.

Qimai Li, Zhichao Han, and Xiao-Ming Wu. Deeper insights into graph convolutional networks for semi-supervised learning. In *Thirty-Second AAAI conference on artificial intelligence*, 2018.

Zhuang Liu, Hanzi Mao, Chao-Yuan Wu, Christoph Feichtenhofer, Trevor Darrell, and Saining Xie. A convnet for the 2020s. In *Proceedings of the IEEE/CVF Conference on Computer Vision and Pattern Recognition*, pp. 11976–11986, 2022.

Ziqi Liu, Chaochao Chen, Longfei Li, Jun Zhou, Xiaolong Li, and Le Song. Geniepath: Graph neural networks with adaptive receptive paths. *Proceedings of the AAAI Conference on Artificial Intelligence*, 33, 02 2018. doi: 10.1609/aaai.v33i01.33014424.

Haggai Maron, Heli Ben-Hamu, Nadav Shamir, and Yaron Lipman. Invariant and equivariant graph networks. *ICLR*, 2018.

Haggai Maron, Heli Ben-Hamu, Hadar Serviansky, and Yaron Lipman. Provably powerful graph networks. *Advances in neural information processing systems*, 32, 2019.

Yimeng Min, Frederik Wenkel, and Guy Wolf. Scattering gcn: Overcoming oversmoothness in graph convolutional networks. *Advances in Neural Information Processing Systems*, 33:14498–14508, 2020.

Federico Monti, Davide Boscaini, Jonathan Masci, Emanuele Rodola, Jan Svoboda, and Michael M Bronstein. Geometric deep learning on graphs and manifolds using mixture model cnns. In *Proceedings of the IEEE Conference on Computer Vision and Pattern Recognition*, pp. 5115–5124, 2017.

Christopher Morris, Martin Ritzert, Matthias Fey, William L Hamilton, Jan Eric Lenssen, Gaurav Rattan, and Martin Grohe. Weisfeiler and leman go neural: Higher-order graph neural networks. In *Proceedings of the AAAI conference on artificial intelligence*, volume 33, pp. 4602–4609, 2019.

Christopher Morris, Nils M. Kriege, Franka Bause, Kristian Kersting, Petra Mutzel, and Marion Neumann. Tudataset: A collection of benchmark datasets for learning with graphs. In *ICML 2020 Workshop on Graph Representation Learning and Beyond (GRL+ 2020)*, 2020. URL www.graphlearning.io.

Marion Neumann, Roman Garnett, Christian Bauckhage, and Kristian Kersting. Propagation kernels: efficient graph kernels from propagated information. *Machine Learning*, 102(2):209–245, 2016.

Kenta Oono and Taiji Suzuki. Graph neural networks exponentially lose expressive power for node classification. In *International Conference on Learning Representations*, 2020. URL <https://openreview.net/forum?id=S1ldO2EFPr>.

Lawrence Page, Sergey Brin, Rajeev Motwani, and Terry Winograd. The pagerank citation ranking: Bringing order to the web. Technical report, Stanford InfoLab, 1999.

Adam Paszke, Sam Gross, Francisco Massa, Adam Lerer, James Bradbury, Gregory Chanan, Trevor Killeen, Zeming Lin, Natalia Gimelshein, Luca Antiga, Alban Desmaison, Andreas Kopf, Edward Yang, Zachary DeVito, Martin Raison, Alykhan Tejani, Sasank Chilamkurthy, Benoit Steiner, Lu Fang, Junjie Bai, and Soumith Chintala. Pytorch: An imperative style, high-performance deep learning library. In H. Wallach, H. Larochelle, A. Beygelzimer, F. d’Alché-Buc, E. Fox, and R. Garnett (eds.), *Advances in Neural Information Processing Systems 32*, pp. 8024–8035. Curran Associates, Inc., 2019. URL <http://papers.neurips.cc/paper/9015-pytorch-an-imperative-style-high-performance-deep-learning-library.pdf>.

Hongbin Pei, Bingzhe Wei, Kevin Chen-Chuan Chang, Yu Lei, and Bo Yang. Geom-gcn: Geometric graph convolutional networks. In *International Conference on Learning Representations*, 2020. URL <https://openreview.net/forum?id=S1e2agrFvS>.

Yu Rong, Wenbing Huang, Tingyang Xu, and Junzhou Huang. Dropedge: Towards deep graph convolutional networks on node classification. In *International Conference on Learning Representations*, 2020. URL <https://openreview.net/forum?id=Hkx1qkrKPr>.

Benedek Rozemberczki, Carl Allen, and Rik Sarkar. Multi-Scale Attributed Node Embedding. *Journal of Complex Networks*, 9(2), 2021.

T Konstantin Rusch, Benjamin P Chamberlain, James Rowbottom, Siddhartha Mishra, and Michael M Bronstein. Graph-coupled oscillator networks. *arXiv preprint arXiv:2202.02296*, 2022.

Mark Sandler, Andrew Howard, Menglong Zhu, Andrey Zhmoginov, and Liang-Chieh Chen. MobileNetV2: Inverted residuals and linear bottlenecks. In *Proceedings of the IEEE Conference on Computer Vision and Pattern Recognition*, pp. 4510–4520, 2018.

Prithviraj Sen, Galileo Namata, Mustafa Bilgic, Lise Getoor, Brian Galligher, and Tina Eliassi-Rad. Collective classification in network data. *AI magazine*, 29(3):93–93, 2008.

Nino Shervashidze, SVN Vishwanathan, Tobias Petri, Kurt Mehlhorn, and Karsten Borgwardt. Efficient graphlet kernels for large graph comparison. In *Artificial intelligence and statistics*, pp. 488–495. PMLR, 2009.

Nino Shervashidze, Pascal Schweitzer, Erik Jan Van Leeuwen, Kurt Mehlhorn, and Karsten M Borgwardt. Weisfeiler-lehman graph kernels. *Journal of Machine Learning Research*, 12(9), 2011.

Christian Szegedy, Sergey Ioffe, Vincent Vanhoucke, and Alexander A Alemi. Inception-v4, inception-resnet and the impact of residual connections on learning. In *Thirty-First AAAI Conference on Artificial Intelligence*, 2017.

Mingxing Tan and Quoc Le. Efficientnet: Rethinking model scaling for convolutional neural networks. In *International conference on machine learning*, pp. 6105–6114. PMLR, 2019.

Matthew Thorpe, Tan Minh Nguyen, Hedi Xia, Thomas Strohmer, Andrea Bertozzi, Stanley Osher, and Bao Wang. GRAND++: Graph neural diffusion with a source term. In *International Conference on Learning Representations*, 2022. URL <https://openreview.net/forum?id=EMxu-dzvJk>.

Petar Veličković, Guillem Cucurull, Arantxa Casanova, Adriana Romero, Pietro Liò, and Yoshua Bengio. Graph Attention Networks. *International Conference on Learning Representations*, 2018. URL <https://openreview.net/forum?id=rJXMpikCZ>.

Guangtao Wang, Rex Ying, Jing Huang, and Jure Leskovec. Improving graph attention networks with large margin-based constraints. *arXiv preprint arXiv:1910.11945*, 2019.

Yue Wang, Yongbin Sun, Ziwei Liu, Sanjay E Sarma, Michael M Bronstein, and Justin M Solomon. Dynamic graph cnn for learning on point clouds. *arXiv preprint arXiv:1801.07829*, 2018.

David P. Williamson. Lecture notes in spectral graph theory course. <https://people.orie.cornell.edu/dpw/orie6334/Fall2016/lecture7.pdf>, 2016.

Felix Wu, Amauri Souza, Tianyi Zhang, Christopher Fifty, Tao Yu, and Kilian Weinberger. Simplifying graph convolutional networks. In *International conference on machine learning*, pp. 6861–6871. PMLR, 2019.

Keyulu Xu, Chengtao Li, Yonglong Tian, Tomohiro Sonobe, Ken-ichi Kawarabayashi, and Stefanie Jegelka. Representation learning on graphs with jumping knowledge networks. In Jennifer Dy and Andreas Krause (eds.), *Proceedings of the 35th International Conference on Machine Learning*, volume 80 of *Proceedings of Machine Learning Research*, pp. 5453–5462. PMLR, 10–15 Jul 2018. URL <http://proceedings.mlr.press/v80/xu18c.html>.

Keyulu Xu, Weihua Hu, Jure Leskovec, and Stefanie Jegelka. How powerful are graph neural networks? In *International Conference on Learning Representations*, 2019. URL <https://openreview.net/forum?id=ryGs6iA5Km>.

Zhilin Yang, William Cohen, and Ruslan Salakhudinov. Revisiting semi-supervised learning with graph embeddings. In *International conference on machine learning*, pp. 40–48. PMLR, 2016.

Jiaxuan You, Jonathan M Gomes-Selman, Rex Ying, and Jure Leskovec. Identity-aware graph neural networks. In *Proceedings of the AAAI Conference on Artificial Intelligence*, volume 35, pp. 10737–10745, 2021.

Jiani Zhang, Xingjian Shi, Junyuan Xie, Hao Ma, Irwin King, and Dit-Yan Yeung. Gaan: Gated attention networks for learning on large and spatiotemporal graphs. In *Proceedings of the Thirty-Fourth Conference on Uncertainty in Artificial Intelligence*, pp. 339–349, 2018a.

Muhan Zhang, Zhicheng Cui, Marion Neumann, and Yixin Chen. An end-to-end deep learning architecture for graph classification. In *Thirty-second AAAI conference on artificial intelligence*, 2018b.

Lingxiao Zhao and Leman Akoglu. Pairnorm: Tackling oversmoothing in gnns. In *International Conference on Learning Representations*, 2020. URL <https://openreview.net/forum?id=rkecl1rtwB>.

Kaixiong Zhou, Xiao Huang, Daochen Zha, Rui Chen, Li Li, Soo-Hyun Choi, and Xia Hu. Dirichlet energy constrained learning for deep graph neural networks. *Advances in Neural Information Processing Systems*, 34, 2021.

Jiong Zhu, Yujun Yan, Lingxiao Zhao, Mark Heimann, Leman Akoglu, and Danai Koutra. Beyond homophily in graph neural networks: Current limitations and effective designs. *Advances in Neural Information Processing Systems*, 33:7793–7804, 2020.

A PROOFS OF THEOREMS

Here we repeat the theorems, observations and corollaries from the main paper, for convenience, and provide their proofs or derivation.

$\tilde{\mathbf{P}}$ is a scaled diffusion operator. Assume that \mathbf{A} is the adjacency matrix, and \mathbf{D} is the degree matrix. Denote the adjacency matrix with added self-loops by $\tilde{\mathbf{A}} = \mathbf{A} + \mathbf{I}$. Then, the convolution operator from GCN (Kipf & Welling, 2016) is

$$\tilde{\mathbf{P}} = \tilde{\mathbf{D}}^{-\frac{1}{2}} \tilde{\mathbf{A}} \tilde{\mathbf{D}}^{-\frac{1}{2}} \quad (12)$$

We first note that the Laplacian including self loops is the same as the regular Laplacian:

$$\tilde{\mathbf{L}} = \tilde{\mathbf{D}} - \tilde{\mathbf{A}} = \mathbf{D} + \mathbf{I} - \mathbf{A} - \mathbf{I} = \mathbf{D} - \mathbf{A} = \mathbf{L}. \quad (13)$$

Therefore, it holds that:

$$\begin{aligned} \tilde{\mathbf{P}} &= \mathbf{I} - \mathbf{I} + \tilde{\mathbf{D}}^{-\frac{1}{2}} \tilde{\mathbf{A}} \tilde{\mathbf{D}}^{-\frac{1}{2}} \\ &= \mathbf{I} - \tilde{\mathbf{D}}^{-\frac{1}{2}} \tilde{\mathbf{D}} \tilde{\mathbf{D}}^{-\frac{1}{2}} + \tilde{\mathbf{D}}^{-\frac{1}{2}} \tilde{\mathbf{A}} \tilde{\mathbf{D}}^{-\frac{1}{2}} \\ &= \mathbf{I} - \tilde{\mathbf{D}}^{-\frac{1}{2}} (\tilde{\mathbf{D}} - \tilde{\mathbf{A}}) \tilde{\mathbf{D}}^{-\frac{1}{2}} \\ &= \mathbf{I} - \tilde{\mathbf{D}}^{-\frac{1}{2}} (\mathbf{D} - \mathbf{A}) \tilde{\mathbf{D}}^{-\frac{1}{2}} \\ &= \mathbf{I} - \tilde{\mathbf{D}}^{-\frac{1}{2}} \mathbf{L} \tilde{\mathbf{D}}^{-\frac{1}{2}}. \end{aligned} \quad (14)$$

Theorem 1. Consider the L times application of equation 7 from the main paper, i.e., $\mathbf{f}^{(L)} = (\tilde{\mathbf{P}}_\omega)^L \mathbf{f}^{(0)}$ with a shared parameter $\omega^{(l)} = \omega$ that is used in all the layers. Also assume that there is some optimal Dirichlet energy of the final feature map that satisfies $0 < E_{opt}(\mathbf{f}^{(L)}) < E(\mathbf{f}^{(0)})$. Then, at the limit, as more layers are added, ω converges to $\bar{\omega}/L$ up to first order accuracy, where L is the number of layers and $\bar{\omega}$ is a value that is independent of L and leads to E_{opt} .

Proof. First, note that equation 6 from the main paper can be written as

$$E(\mathbf{f}^{(l)}) = \sum_{i \in \mathcal{V}} \sum_{j \in \mathcal{N}_i} \frac{1}{2} \left\| \frac{\mathbf{f}_i^{(l)}}{\sqrt{(1+d_i)}} - \frac{\mathbf{f}_j^{(l)}}{\sqrt{(1+d_j)}} \right\|_2^2 = \frac{1}{2} \|\mathbf{G} \tilde{\mathbf{D}}^{-\frac{1}{2}} \mathbf{f}^{(l)}\|_2^2, \quad (15)$$

where \mathbf{G} is the graph gradient operator, also known as the incidence matrix, that for each edge subtracts the features of the two connected nodes, i.e., $\mathbf{G} \mathbf{f}_{(i,j)}^{(l)} = \mathbf{f}_i^{(l)} - \mathbf{f}_j^{(l)}$ for $(i, j) \in \mathcal{E}$. Let us assume that the initial feature $\mathbf{f}^{(0)}$ has some Dirichlet energy $E_0 > E_{opt}$ as defined in equation 15. Since

$$\nabla E = \tilde{\mathbf{D}}^{-\frac{1}{2}} \mathbf{G}^\top \mathbf{G} \tilde{\mathbf{D}}^{-\frac{1}{2}} \mathbf{f}^{(l)}$$

we see that the forward propagation through a GCN approximates the gradient flow of the Dirichlet energy. That is, for given L and ω we have that

$$\mathbf{f}^{(l+1)} = \mathbf{f}^{(l)} - \omega \nabla E = \mathbf{f}^{(l)} - \omega \tilde{\mathbf{D}}^{-\frac{1}{2}} \mathbf{G}^\top \mathbf{G} \tilde{\mathbf{D}}^{-\frac{1}{2}} \mathbf{f}^{(l)} = (\mathbf{I} - \omega \tilde{\mathbf{D}}^{-\frac{1}{2}} \mathbf{L} \tilde{\mathbf{D}}^{-\frac{1}{2}}) \mathbf{f}^{(l)} \quad (16)$$

where we used that $\mathbf{G}^\top \mathbf{G} = \mathbf{L}$. Equation 16 can be seen both as a gradient descent step to reduce E , and also as a forward Euler approximation with step size ω of the solution of

$$\frac{\partial \mathbf{f}(t)}{\partial t} = -\tilde{\mathbf{D}}^{-\frac{1}{2}} \mathbf{L} \tilde{\mathbf{D}}^{-\frac{1}{2}} \mathbf{f}(t), \quad \mathbf{f}(0) = \mathbf{f}^{(0)}. \quad (17)$$

It is known that the solution to equation 17 is given by

$$\mathbf{f}(t) = \exp \left(-t \tilde{\mathbf{D}}^{-\frac{1}{2}} \mathbf{L} \tilde{\mathbf{D}}^{-\frac{1}{2}} \right) \mathbf{f}(0). \quad (18)$$

Since the Dirichlet energy of $\mathbf{f}(t)$ is continuous in t and decays monotonically from E_0 to zero, there exists a T such that $E(\mathbf{f}(T)) = E_{opt}$. Now, considering discrete time intervals $0 = t_0, \dots, t_L = T$, then, similarly to equation 18, for any two subsequent time steps t_{l+1} and t_l we have that

$$\mathbf{f}(t_{l+1}) = \exp \left(-(t_{l+1} - t_l) \tilde{\mathbf{D}}^{-\frac{1}{2}} \mathbf{L} \tilde{\mathbf{D}}^{-\frac{1}{2}} \right) \mathbf{f}(t_l). \quad (19)$$

Taking fixed-interval time steps such that $t_{l+1} - t_l = \omega = T/L$ for $l = 0, \dots, L$, we get

$$\mathbf{f}(t_{l+1}) = \exp\left(-\omega\tilde{\mathbf{D}}^{-\frac{1}{2}}\mathbf{L}\tilde{\mathbf{D}}^{-\frac{1}{2}}\right)\mathbf{f}(t_l) = (\mathbf{I} - \omega\tilde{\mathbf{D}}^{-\frac{1}{2}}\mathbf{L}\tilde{\mathbf{D}}^{-\frac{1}{2}})\mathbf{f}(t_l) + O(\omega^2), \quad (20)$$

where the rightmost approximation holds due to the Taylor expansion up to first order approximation. Denoting $\mathbf{f}^{(l)} = \mathbf{f}(t_l)$ and $\bar{\omega} = T$, we complete the proof. \square

Corollary 1. *Allowing a variable $\omega^{(l)} > 0$ in Theorem 1, yields $\sum_{l=0}^{L-1} \omega^{(l)} = \bar{\omega}$ up to first order accuracy.*

Proof. The proof follows immediately by setting variable $t_{l+1} - t_l = \omega^{(l)}$ and placing in equation 20. \square

Remark 1 (The non-negativity of $\tilde{\mathbf{P}}_\omega$). *By definition, for $0 < \omega \leq 1$ all the spatial weights of $\tilde{\mathbf{P}}_\omega$ defined in equation 7 are non-negative, and it is that the operator is smoothing as it is a low-pass filter. For $\omega > 1$ or $\omega < 0$, by definition we have an operator with mixed signs.*

Theorem 2. *Assume that the graph is connected. Then, there exists some $\omega_0 \geq 1$ where for all $0 < \omega < \omega_0$, the operator $\tilde{\mathbf{P}}_\omega$ in equation 7 from the main paper is smoothing and the leading eigenvector is $\tilde{\mathbf{D}}^{\frac{1}{2}}\mathbf{1}$. For $\omega > \omega_0$ or $\omega < 0$, the leading eigenvector changes.*

Proof. Assuming that the graph is connected, it is known that the graph Laplacian matrix has the eigenvector $\mathbf{1}$ whose eigenvalue is 0, i.e. $\mathbf{L}\mathbf{1} = 0$. Hence, we get that $\tilde{\mathbf{D}}^{-\frac{1}{2}}\mathbf{L}\tilde{\mathbf{D}}^{-\frac{1}{2}}\tilde{\mathbf{D}}^{\frac{1}{2}}\mathbf{1} = 0$ so $\tilde{\mathbf{D}}^{\frac{1}{2}}\mathbf{1}$ is the eigenvector of the normalized Laplacian with eigenvalue of 0.

Furthermore, denote the normalized Laplacian by $\tilde{\mathbf{L}} = \tilde{\mathbf{D}}^{-\frac{1}{2}}\mathbf{L}\tilde{\mathbf{D}}^{-\frac{1}{2}}$. Consider the range

$$0 < \omega < \frac{2}{\rho(\tilde{\mathbf{L}})} = \omega_0,$$

where $\rho(\tilde{\mathbf{L}})$ denotes the spectral radius of the matrix $\tilde{\mathbf{L}}$. It is easy to verify that for this range of values for ω , the largest eigenvalue in magnitude of $\tilde{\mathbf{P}}_\omega$ is 1, and it corresponds to the null eigenvector of $\tilde{\mathbf{L}}$, i.e., $\tilde{\mathbf{D}}^{\frac{1}{2}}\mathbf{1}$. Hence, for this range, $\tilde{\mathbf{P}}$ is smoothing. For $\omega > \omega_0$ and $\omega < 0$, the leading eigenvector of $\tilde{\mathbf{P}}_\omega$ becomes the leading eigenvector of $\tilde{\mathbf{L}}$. Furthermore, it can be shown that $\rho(\tilde{\mathbf{L}}) \leq 2$ (see Williamson (2016) for the proof), hence $\omega_0 \geq 1$. \square

B SYNTHETIC EXPRESSIVENESS TASK

To demonstrate the importance and benefit of learning sharpening propagation operators in addition to smoothing operators, we propose the following synthetic node gradient regression task. Given a graph $\mathcal{G} = (\mathcal{V}, \mathcal{E})$ with some input node features $\mathbf{f}^{in} \in \mathbb{R}^{n \times c_{in}}$, we wish a GNN to regress the node features gradient, $\nabla \mathbf{f}^{in}$, where the node feature gradient of the i -th node is defined as an upwind gradient operator:

$$\nabla \mathbf{f}_i^{in} = \max_{j \in \mathcal{N}_i} (\mathbf{f}_i - \mathbf{f}_j), \quad (21)$$

where the goal of the considered GNN is to minimize the following objective:

$$\|\text{GNN}(\mathbf{f}^{in}, \mathcal{G}) - \nabla \mathbf{f}^{in}\|_2^2. \quad (22)$$

As a comparison, we consider two GNNs: GCN (Kipf & Welling, 2016) and our ω GCN with 64 channels and 2 layers. In both cases we use a learning rate of $1e-4$ without weight decay and train the network for 5000 iterations (no further benefit was obtained with any of the considered methods). The input graph is a random Erdős–Rényi graph with 8 nodes and an edge rate of 30%, with input node features sampled from a uniform distribution in the range of 0 to 1. The obtained loss of GCN is of order $1e-1$, while our ω GCN obtains a loss of order $1e-12$, also as can be seen in Fig. 2. We therefore conclude that introducing the ability of learning mixed-sign operators by ω is beneficial to enhance the expressiveness of GNNs.

C DATASETS

In this section we provide the statistics of the datasets used throughout our experiments. Tab. 8 presents information regarding node-classification datasets, and Tab. 9 summarizes the graph-classification datasets. For each dataset, we also provide the homophily score as defined by Pei et al. (2020).

Table 8: Node classification datasets statistics. Hom. score denotes the homophily score.

Dataset	Cora	Citeseer	Pubmed	Chameleon	Actor (Film)	Cornell	Texas	Wisconsin	PPI	Ogbn-arxiv
Classes	7	6	3	5	5	5	5	5	121	40
Nodes	2,708	3,327	19,717	2,277	7,600	183	183	251	56,944	169,343
Edges	5,429	4,732	44,338	36,101	33,544	295	309	499	818,716	1,116,243
Features	1,433	3,703	500	2,325	932	1,703	1,703	1,703	50	128
Hom. score	0.81	0.80	0.74	0.23	0.22	0.30	0.11	0.21	0.17	0.63

Table 9: TUDatasets graph classification statistics.

Dataset	MUTAG	PTC	PROTEINS	NCI1	NCI109
Classes	2	2	2	2	2
Graphs	188	344	1113	4110	4127
Avg. nodes	17.93	14.29	39.06	29.87	32.13
Avg. edges	19.79	14.69	72.82	32.30	32.13

D OVER-SMOOTHING IN GAT

In addition to the observation presented in Sec. 2.1 and specifically in Fig. 3b where we see that recurrent applications of GAT reduces the node feature energy from equation 11, which causes over-smoothing as shown by Wu et al. (2019); Wang et al. (2019) (as discussed in the main paper), here, we also show that the same behaviour is evident with Citeseer and Pubmed datasets in Fig. 5.

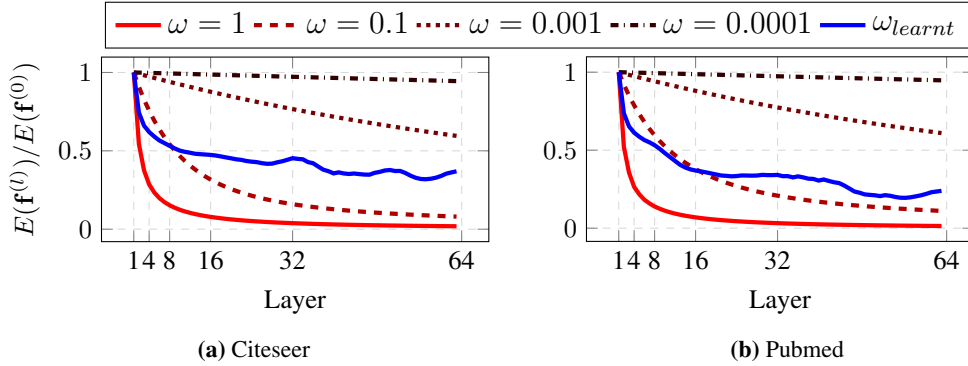


Figure 5: Node features energy at the l -th layer relative to the initial node embedding energy on Citeseer 5a and Pubmed 5b. ω GAT controls the energy from Eq. equation 11 to avoid over-smoothing, while the baseline GAT with $\omega = 1$ reduce the energy to 0 and over-smooth.

E ARCHITECTURES IN DETAILS

We now elaborate on the specific architectures used in our experiments in Sec. 4. As noted in the main paper, all our network architectures consist of an opening (embedding) layer (1×1 convolution), a sequence of ω GNN (i.e., ω GCN or ω GAT) layers, and a closing (classifier) layer (1×1 convolution). In total, we have two types of architectures – one that is based on GCN, for node classification tasks

reported in Tab. 10, and the other for the graph classification task which is based on Xu et al. (2019) and is reported in Tab. 11. Throughout the following, we denote by c_{in} and c_{out} the input and output channels, respectively, and c denotes the number of features in hidden layers (which is a reported in Appendix F). We initialize the embedding and classifier layers with the Glorot (Glorot & Bengio, 2010) initialization, and $\mathbf{K}^{(l)}$ from equation 2 is initialized with an identity matrix of shape $c \times c$. The initialization of $\Omega^{(l)}$ also starts from a vectors of ones. We note that our initialization yields a standard smoothing process, which is then adapted to the data as the learning process progresses, and if needed also changes the process to a non-smoothing one by the means of mixed-signs, as discussed earlier and specifically in Theorem. 2. We denote the number of ω GNN layers by L , and the dropout probability by p . The main difference between the two architectures are as follows. First, for the graph classification we use the standard add-pool operation as in GIN (Xu et al., 2019) to obtain a global graph feature. Second, we follow GIN and in addition to the graph layer (which is ω GNN in our work), we add batch normalization (denoted by BN), 1×1 convolution and a ReLU activation past each graph layer.

Table 10: The architecture used for node classification and inductive learning.

Input size	Layer	Output size
$n \times c_{in}$	1×1 Dropout(p)	$n \times c_{in}$
$n \times c_{in}$	1×1 Convolution	$n \times c$
$n \times c$	ReLU	$n \times c$
$n \times c$	$L \times \omega$ GNN layers	$n \times c$
$n \times c$	1×1 Dropout(p)	$n \times c$
$n \times c$	1×1 Convolution	$n \times c_{out}$

Table 11: The architecture used for graph classification.

Input size	Layer	Output size
$n \times c_{in}$	1×1 Convolution	$n \times c$
$n \times c$	ReLU	$n \times c$
$n \times c$	$L \times [\omega$ GNN, BN, 1×1 Convolution, ReLU]	$n \times c$
$n \times c$	1×1 Add-pool	$1 \times c$
$1 \times c$	1×1 Convolution	$1 \times c$
$1 \times c$	1×1 Dropout(p)	$1 \times c$
$1 \times c$	1×1 Convolution	$1 \times c_{out}$

F HYPER-PARAMETERS DETAILS

We provide the selected hyper-parameters in our experiments. We denote the learning rate of our ω GNN layers by LR_{GNN} , and the learning rate of the 1×1 opening and closing as well as any additional classifier layers by LR_{oc} . Also, the weight decay for the opening and closing layers is denoted by WD_{oc} . We denote the ω parameter learning rate and weight decay by LR_{ω} and WD_{ω} , respectively. c denotes the number of hidden channels. In the case of ω GAT, the attention head vector \mathbf{a} are learnt with the same learning rate as LR_{GNN} and WD_{GNN} .

F.1 SEMI-SUPERVISED NODE CLASSIFICATION

The hyper-parameters for this experiment are summarized in Tab. 12.

F.2 FULL-SUPERVISED NODE CLASSIFICATION

The hyper-parameters for this experiment are summarized in Tab. 13. The number of layers used in Tab. 3 are mentioned in brackets in the table. For Ogbn-arxiv and Actor from Tab. 4, 8 layer ω GCN and ω GAT were employed.

Table 12: Semi-supervised node classification hyper-parameters.

Architecture	Dataset	LR_{GNN}	LR_{oc}	LR_{ω}	WD_{GNN}	WD_{oc}	WD_{ω}	c	p
ω GCN	Cora	0.01	0.01	0.01	1e-4	8e-5	2e-4	64	0.6
	Citeseer	1e-4	0.005	0.005	1e-5	5e-6	2e-4	256	0.7
	Pubmed	0.001	5e-4	0.005	2e-4	1e-4	1e-4	256	0.5
ω GAT	Cora	0.01	0.01	0.005	1e-5	1e-5	1e-5	64	0.6
	Citeseer	0.005	0.005	0.001	1e-4	1e-5	1e-4	256	0.7
	Pubmed	0.005	0.001	0.05	4e-5	1e-5	1e-4	256	0.5

F.3 INDUCTIVE LEARNING

The hyper-parameters for the inductive learning on PPI are listed in Sec. 4.3 in the main paper, and are the same for ω GCN and ω GAT.

Table 13: Full-supervised node classification hyper-parameters.

Architecture	Dataset	LR_{GNN}	LR_{oc}	LR_{ω}	WD_{GNN}	WD_{oc}	WD_{ω}	c	p
ω GCN	Cora	0.01	0.05	0.005	0.01	1e-4	1e-4	64	0.5
	Citeseer	0.001	0.08	0.005	0.005	1e-4	0	64	0.5
	Pubmed	0.005	0.005	0.01	0.003	5e-5	0.01	64	0.5
	Chameleon	1e-4	0.005	5e-4	1e-4	1e-4	1e-5	64	0.5
	Actor (Film)	0.05	0.01	0.05	1e-4	1e-4	1e-5	64	0.5
	Cornell	0.01	0.05	0.01	0.005	1e-4	0	64	0.5
	Texas	0.08	0.08	0.005	0.005	5e-4	0	64	0.5
	Wisconsin	0.001	0.05	0.005	1e-4	3e-4	3e-4	64	0.5
	Ogbn-arxiv	0.01	0.01	0.01	0	0	0	256	0
ω GAT	Cora	0.001	0.01	0.05	0.001	5e-4	0	64	0.5
	Citeseer	0.005	0.05	0.03	0.005	5e-4	0.001	64	0.5
	Pubmed	0.05	0.005	0.005	0.003	1e-6	0.003	64	0.5
	Chameleon	0.005	0.005	3e-4	5e-4	5e-4	1e-5		
	Actor (Film)	0.05	0.01	0.01	5e-4	0.001	4e-4	64	0.5
	Cornell	0.001	0.01	0.005	1e-4	1e-5	0	64	0.5
	Texas	1e-4	0.02	0.05	5e-4	5e-4	0	64	0.5
	Wisconsin	0.01	0.05	0.005	0.001	5e-4	0	64	0.5
	Ogbn-arxiv	0.01	0.01	0.01	0	0	0	256	0

F.4 GRAPH CLASSIFICATION

The hyper-parameters for the graph classification experiment on TUDatasets are reported in Tab. 14. We followed the same grid-search procedure as in GIN (Xu et al., 2019). In all experiment, a 5 layer (including the initial embedding layer) ω GCN and ω GAT are used, similarly to GIN.

F.5 ABLATION STUDY

In this experiment we used the same hyper-parameters as reported in Tab. 12.

G RUNTIMES

Following the computational cost discussion from Sec. 2.4 in the main paper, we also present in Tab. 15 the measured training and inference times of our baselines GCN and GAT with 2 layers, where we see that indeed the addition of ω per layer and channel requires a negligible addition of time, at the return of a significantly more accurate GNN. We note that further accuracy gain can be achieved

Table 14: Graph classification hyper-parameters. BS denoted batch size.

Architecture	Dataset	LR_{GNN}	LR_{oc}	LR_{ω}	WD_{GNN}	WD_{oc}	WD_{ω}	c	p	BS
ω GCN	MUTAG	0.01	0.01	0.01	0	0	0	32	0	32
	PTC	0.01	0.01	0.01	0	0	0	32	0	32
	PROTEINS	0.01	0.01	0.01	0	0	0	32	0	128
	NCI1	0.01	0.01	0.01	0	0	0	32	0.5	32
	NCI109	0.01	0.01	0.01	0	0	0	32	0	32
ω GAT	MUTAG	0.01	0.01	0.01	0	0	0	32	0	32
	PTC	0.01	0.01	0.01	0	0	0	32	0	128
	PROTEINS	0.01	0.01	0.01	0	0	0	32	0	128
	NCI1	0.01	0.01	0.01	0	0	0	32	0.5	128
	NCI109	0.01	0.01	0.01	0	0	0	32	0.5	32

when adding more ω GNN layers as reported in Tab. 2 in the main paper. However, since GCN and GAT over-smooth, the comparison here is done with 2 layers, where the highest accuracy is obtained for the baseline models.

Table 15: Training and inference GPU runtimes [ms] on Cora.

Runtime	GCN	GAT	ω GCN (Ours)	ω GAT (Ours)
Training	7.71	14.59	7.79	14.95
Inference	1.75	2.98	1.88	3.09
Accuracy (%)	81.1	83.1	82.6	83.4

H ABLATION STUDY USING ω GAT

To complement our ablation study on ω GNN in Sec. 4.5 in the main paper, we perform as similar study on ω GAT. Here, we show in Tab. 16, that indeed the single ω variant, dubbed ω GAT_G does not over-smooth, and that by allowing the greater flexibility of a per-layer and per layer and channel of our ω GAT_{PL} and ω GAT, respectively, better performance is obtained.

Table 16: Ablation study on ω GAT.

Data.	Variant	Layers					
		2	4	8	16	32	64
Cora	ω GAT _G	83.3	83.3	83.4	83.6	83.7	83.9
	ω GAT _{PL}	83.4	83.5	83.8	84.0	84.1	84.0
	ω GAT	83.4	83.7	84.0	84.3	84.4	84.8
Cite.	ω GAT _G	71.5	71.8	71.9	72.2	72.4	72.9
	ω GAT _{PL}	72.1	72.3	72.4	72.8	73.1	73.2
	ω GAT	72.5	73.1	73.3	73.5	73.9	74.0
Pub.	ω GAT _G	80.0	80.2	80.3	80.5	80.6	80.9
	ω GAT _{PL}	80.0	80.4	80.7	81.1	81.2	81.4
	ω GAT	80.3	81.0	81.2	81.3	81.5	81.8

Table 17: Semi-supervised node classification test accuracy 100 random train-val-test splits.

Method	Cora	Citeseer	Pubmed
GCN (Kipf & Welling, 2016)	81.5	71.9	77.8
GAT (Veličković et al., 2018)	81.8	71.4	78.7
MoNet (Monti et al., 2017)	81.3	71.2	78.6
GRAND-l (Chamberlain et al., 2021)	83.6	73.4	78.8
GRAND-nl (Chamberlain et al., 2021)	82.3	70.9	77.5
GRAND-nl-rw (Chamberlain et al., 2021)	83.3	74.1	78.1
GraphCON-GCN (Rusch et al., 2022)	81.9	72.9	78.8
GraphCON-GAT (Rusch et al., 2022)	83.2	73.2	79.5
GraphCON-Tran (Rusch et al., 2022)	84.2	74.2	79.4
ω GCN (ours)	84.5	73.8	82.9
ω GAT (ours)	84.3	73.6	82.6

I STATISTICAL SIGNIFICANCE OF SEMI-SUPERVISED NODE CLASSIFICATION RESULTS

Throughout our semi-supervised node classification experiment in Sec. 4 on Cora, Citeseer and Pubmed, the standard split from Kipf & Welling (2016) was considered, to a direct comparison with as many as possible methods. However, since this result reflects the accuracy from a single split, we also repeat this experiment with 100 random splits as in Chamberlain et al. (2021) and compare with applicable methods that also conducted such statistical significance test. In Tab. 17, we report our obtained accuracy on Cora, Citeseer and Pubmed. It is possible to see that in this experiment our ω GCN and ω GAT outperform or obtain similar results compared with the considered methods, which further highlight the performance advantage of our method.

J THE LEARNT $\vec{\omega}$

One of the main advantages of our method in Sec. 2 is that our method is capable of learning both smoothing and sharpening propagation operators, which cannot be obtained in most current GNNs. In Fig. 6 we present the actual $\{\omega^{(l)}\}_{l=1}^L$ as a matrix of size $L \times c$ that was learnt for two dataset of different types—with high and low homophily score (as described in Pei et al. (2020)). Namely, the Cora dataset with a high homophily score of 0.81, and the Texas dataset with a low homophily score of 0.11 (i.e., a heterophilic dataset). We see that a homophilic dataset like Cora, the network learnt to perform diffusion, albeit in a controlled manner, and not to simply employ the standard averaging operator $\tilde{\mathbf{P}}$. We can further see that for a heterophilic dataset the ability to learn contrastive (i.e., sharpening) propagation operators in addition to diffusive kernels is beneficial, and is also reflected in our results in Tab. 3, where a larger improvement is achieved in datasets like Cornell, Texas and Wisconsin, which have low homophily scores (Rusch et al., 2022).

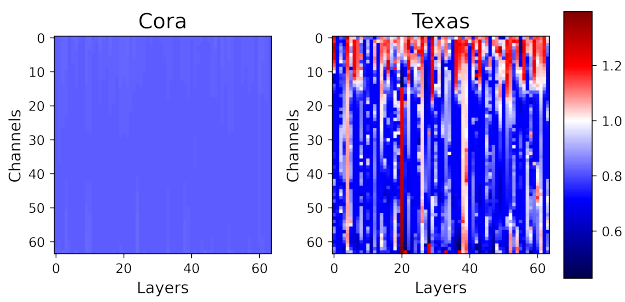


Figure 6: The learnt $\vec{\omega} \in \mathbb{R}^{64 \times 64}$ of ω GCN with 64 layers (x-axis) and 64 channels (y-axis) for Cora (homophilic) and Texas (heterophilic) datasets. Smoothing operators appear in blue, while sharpening operators appear in red. White entries are obtained for $\omega = 1$.